Marquette University
e-Publications@Marquette

Chemistry Faculty Research and Publications

Chemistry, Department of

8-4-2016

First Experimental Evidence for the Diverse Requirements of Excimer vs Hole Stabilization in π-Stacked Assemblies

Neil Reilly
Marquette University

Maxim Vadimovich Ivanov
Marquette University

Brandon Uhler
Marquette University

Marat R. Talipov
Marquette University

Rajendra Rathore
Marquette University

See next page for additional authors

Authors

Neil Reilly, Maxim Vadimovich Ivanov, Brandon Uhler, Marat R. Talipov, Rajendra Rathore, and Scott Reid

First Experimental Evidence for the Diverse Requirements of Excimer vs Hole Stabilization in π-Stacked Assemblies

Neil Reilly
Department of Chemistry, Marquette University, Milwaukee, WI

Maxim Ivanov
Department of Chemistry, Marquette University, Milwaukee, WI

Brandon Uhler
Department of Chemistry, Marquette University, Milwaukee, WI

Marat Talipov
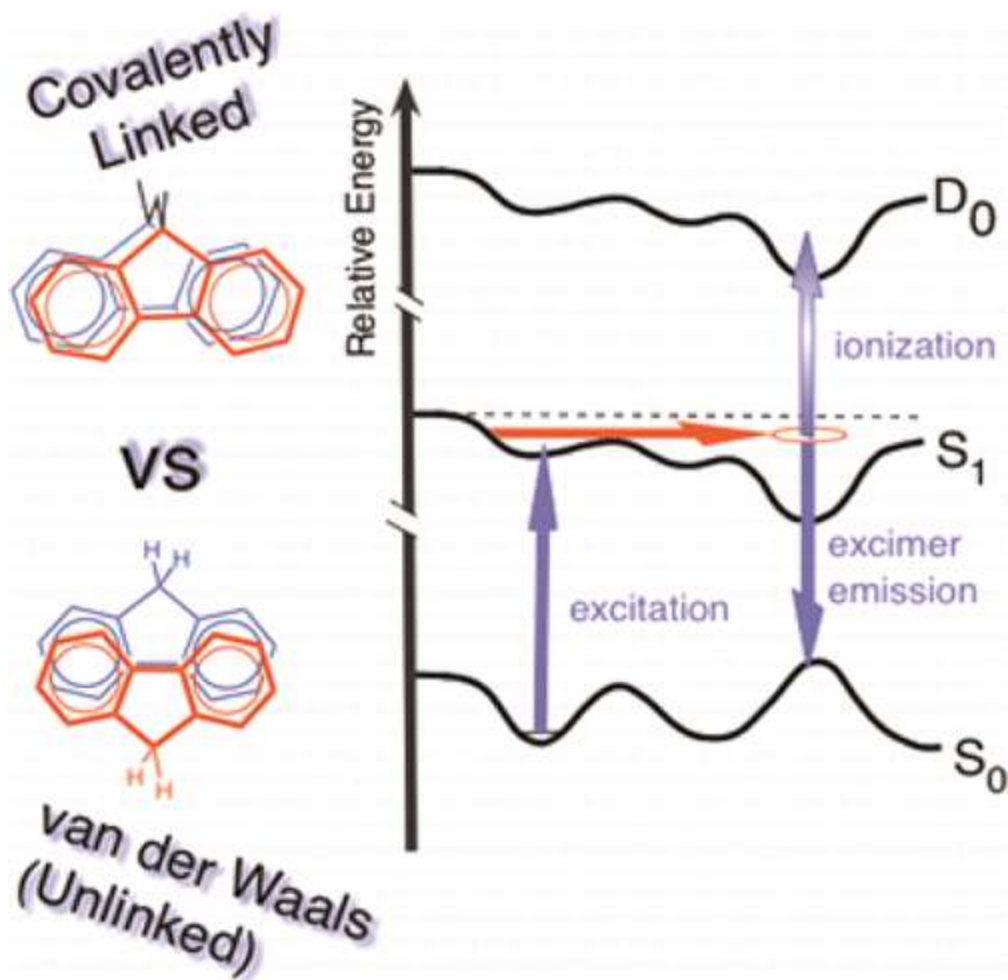*Department of Chemistry, Marquette University, Milwaukee, WI*

Rajendra Rathore
Department of Chemistry, Marquette University, Milwaukee, WI

Scott A. Reid

Department of Chemistry, Marquette University, Milwaukee, WI

Abstract

Exciton formation and charge separation and transport are key dynamical events in a variety of functional polymeric materials and biological systems, including DNA. Beyond the necessary cofacial approach of a pair of aromatic molecules at van der Waals contact, the extent of overlap and necessary geometrical reorganization for optimal stabilization of an excimer vs dimer cation radical remain unresolved. Here, we compare experimentally the

dynamics of excimer formation (via emission) and charge stabilization (via threshold ionization) of a novel covalently linked, cofacially stacked fluorene dimer (F2) with the unlinked van der Waals dimer of fluorene, that is, $(F)_2$. Although the measured ionization potentials are identical, the excimeric state is stabilized by up to ~30 kJ/mol in covalently linked F2. Supported by theory, this work demonstrates for the first time experimentally that optimal stabilization of an excimer requires a perfect sandwich-like geometry with maximal overlap, whereas hole stabilization in π-stacked aggregates is less geometrically restrictive.

The dynamics of exciton and hole formation and migration in π-stacked assemblies are central to the mechanisms of biological systems and the development of functional polymeric materials.[1] As the simplest units capable of excimer formation and charge delocalization, dimers of benzene,[2,3] fluorene,[4,5] naphthalene,[6] and pyrene[7] have served as models for understanding excitonic interactions and electron transfer in multichromophoric assemblies.[8-10] Though it is appreciated that π-stacked assemblies stabilize both charge and excitation energy, the geometrical reorganizations and underlying mechanisms accompanying these important events are not well understood nor, indeed, is there a unified understanding of π-stacking interactions.[11,12]

Representing a significant advance in our ability to study π-stacked aggregates, the Rathore group reported the synthesis and spectroscopic characterization of a novel set of polyfluorenes covalently linked at the 9-position through a single methylene spacer (denoted **Fn**; n = 1–6).[13-17] These molecules adopt a cofacial arrangement in gas, liquid, and solid state and have been utilized as model systems to examine energy and electron transport in π-stacked assemblies.[18] Herein, we use F2 as a model covalently linked system, which we compare with the unlinked (i.e., van der Waals) dimer of fluorene, that is, $(F)_2$ in order to examine the geometrical requirements for excimer vs dimer cation radical stabilization. Utilizing a powerful experimental approach in vacuo which monitors emission or delayed ionization from the excimeric states, we compare emission and resonant ionization spectra of the two dimers, which affords a facile comparison of the relative stabilization of excimer vs hole (i.e., cation radical). We thus probe for the first time the relative efficiency and geometrical requirements of excimer formation vs charge stabilization in a model bichromophore.

A schematic of the experiment is shown in Figure 1. Our studies were carried out on isolated cold ($T_{rot} \sim 20$ K) molecules in the gas-phase using a supersonic nozzle; details are provided in the Supporting Information (SI). In each case, laser excitation from the ground state minimum placed the dimer on the S_1 surface, where rapid rearrangement resulted in excimer formation, evidenced in the dominance of excimer emission and a lengthened fluorescence lifetime. Analysis of line widths in the $(F)_2$ spectrum (Figure S1) indicate a time scale for this process of several picoseconds, consistent with recent studies of the benzene dimer.[19] From the excimeric well, absorption of a photon from a second laser pulse, delayed by $\sim$5 ns, led to ionization; scanning the energy of the second photon while monitoring the mass signature of interest generated an ion yield curve, from which the ionization threshold was extracted.
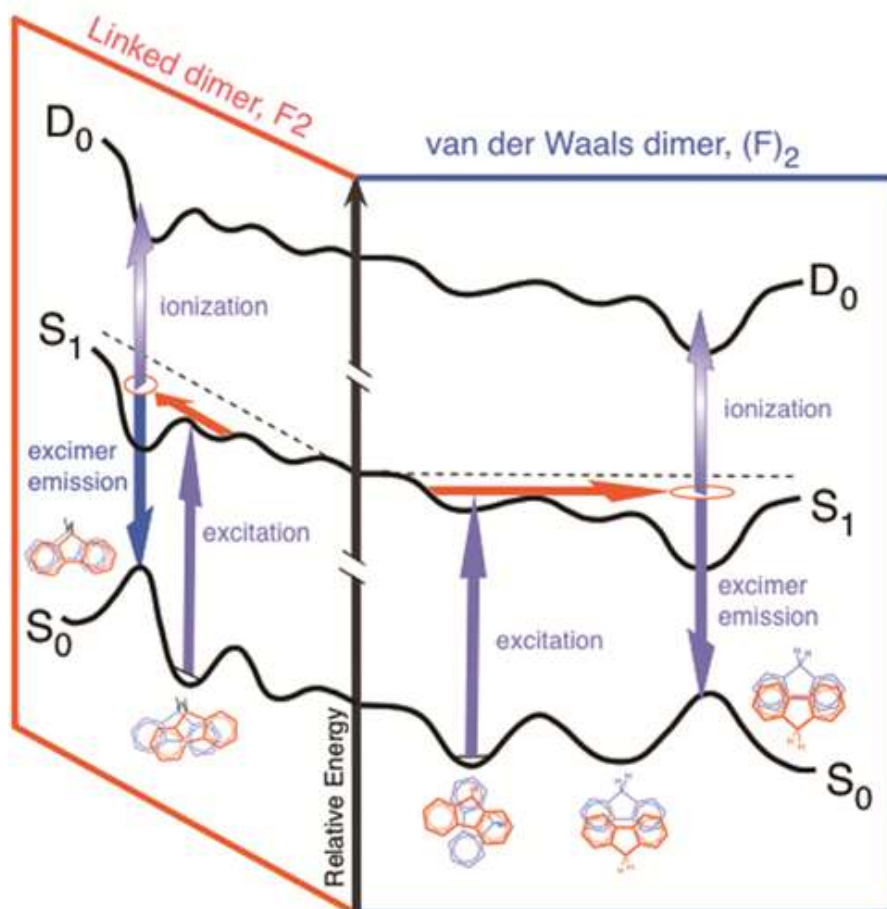

Figure 1. Experimental schematic. For both covalently linked F2 and the van der Waals dimer $(F)_2$, excitation of the isolated dimer leads to rapid excimer formation, which is probed by monitoring emission, or by delayed ionization.

Gas-phase emission spectra of F2 and (F)$_2$ are compared in Figure 2 with the solution phase spectrum of F2, measured in dichloromethane. All spectra show a broad, red-shifted feature characteristic of excimeric emission, and the lifetime of the F2 emission, of order 60 ns, is similar to the reported lifetime (54 ns) of (F)$_2$.[6] However, the position of the F2 emission feature is shifted to longer wavelength by some 40 nm from that of (F)$_2$, indicating significant (up to ~30 kJ/mol) stabilization of the excimer in the covalently linked system. We suggest that this stabilization arises from the ability of the covalently linked dimer to form a perfect sandwich structure, which is not possible in the van der Waals dimer due to steric repulsion. Interestingly, the solution and gas-phase spectra of F2 are similar, revealing little solvochromatic effect.
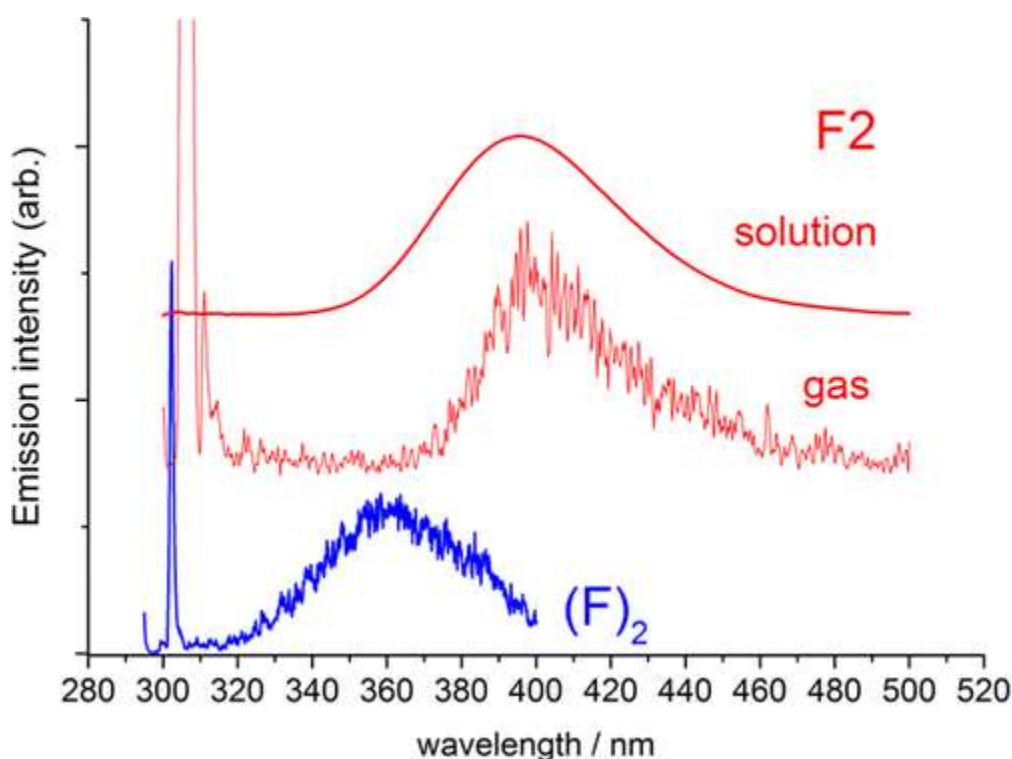
Figure 2. Emission spectra of F2 and (F)$_2$ in the gas phase. Also shown for comparison is the solution phase spectrum of F2.

To probe the degree of stabilization of the cation radicals in the two dimers, ionization thresholds were determined using two-color ionization. Photoionization from the excimer well is expected to show favorable Franck–Condon factors, owing to the similar geometries of excimer and cation radical. However, under our conditions no

collisional relaxation occurs on the time scale of the experiment, and ionization therefore occurs from highly excited vibrational levels in the excimer well, giving rise to a gradual onset in the dimer ion yield curves, shown in Figure 3, which compares ion yield curves for F2 and (F)$_2$ (upper panel) with that of the fluorene monomer. The dimers display identical ionization thresholds of ~7.51(1) eV, significantly lowered by ~0.38 eV or 40 kJ/mol relative to the monomer (7.885(5) eV). Thus, the cation radical state is stabilized in the dimers, as expected, but surprisingly to a *similar* degree. This strongly suggests that, in comparison with excimer formation, stabilization of the cation radical does not require optimum overlap; that is, that the geometrical requirements for hole stabilization are less restrictive.[20] Note that the IP of F2 determined here via two-color ionization is consistent with an prior determination from photoelectron spectroscopy.[13]

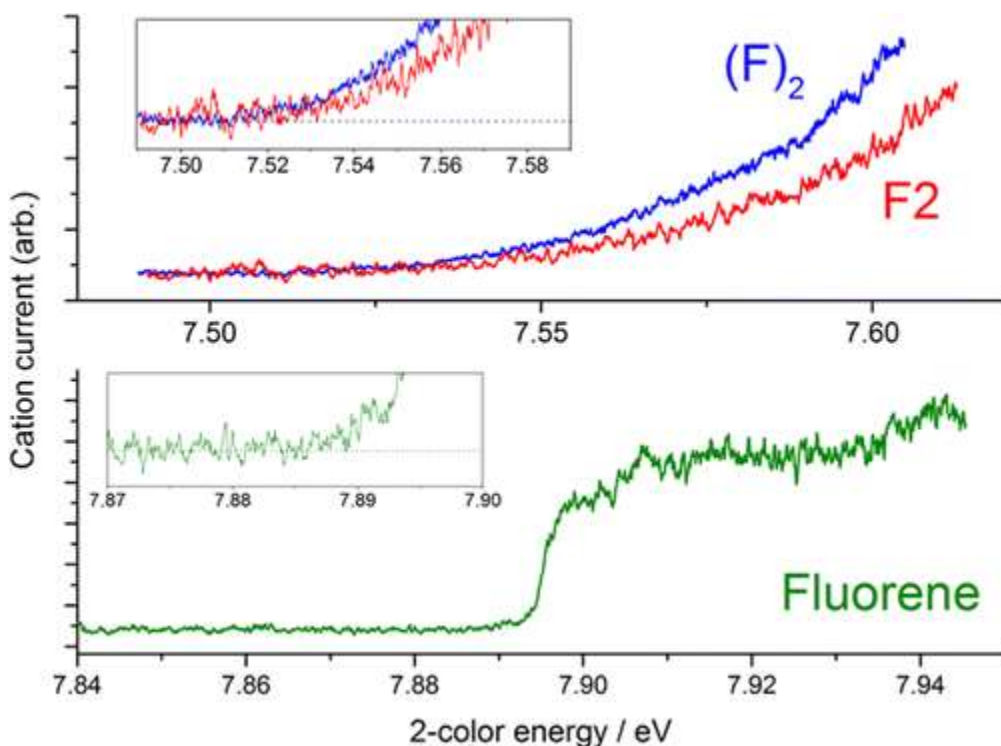
Figure 3. Ion yield curves of (F)$_2$, F2 and fluorene monomer.

Our experimental findings are consistent with computational studies of the relevant potential energy surfaces. Due to the importance of electron correlation in the proper description of π-stacking interactions, we performed a brief benchmarking study of the benzene dimer;[21] details are provided in the SI. We found that

6

accurate energies could be obtained using a simple PBE0 density functional[22,23] augmented with the D3 version of Grimme's dispersion term,[24] at a fraction of the cost of more sophisticated methods (Table S1). Thus, ground state calculations were performed at the PBE0-D3 level with a def2-TZVP basis set.[25,26] Excited electronic states were computed with time-dependent DFT at the PBE0-D3 level with def2-TZVP or def2-SV(P) basis sets. For the cation radical states, a calibrated[27-29] B1LYP functional (B1LYP-40) was employed, with a 6-31G(d) basis set; wave function stability tests were performed to ensure the absence of states with lower energy.

Figure 4 displays the energies of relevant points on the singlet PESs of $(F)_2$, at left, and F2. The global minimum of the van der Waals dimer corresponds to a parallel orthogonal conformer, which is consistent with the experimental finding of excitonic bands bearing nearly equal intensity (Table S2).[5] On the S_1 surface, the head-to-tail sandwich excimer structure is the global minimum, lying ~64 kJ/mol below the vertical energy of the locally excited (LE) state. Vertical ionization requires 333 kJ/mol of energy from the bottom of the excimer well.
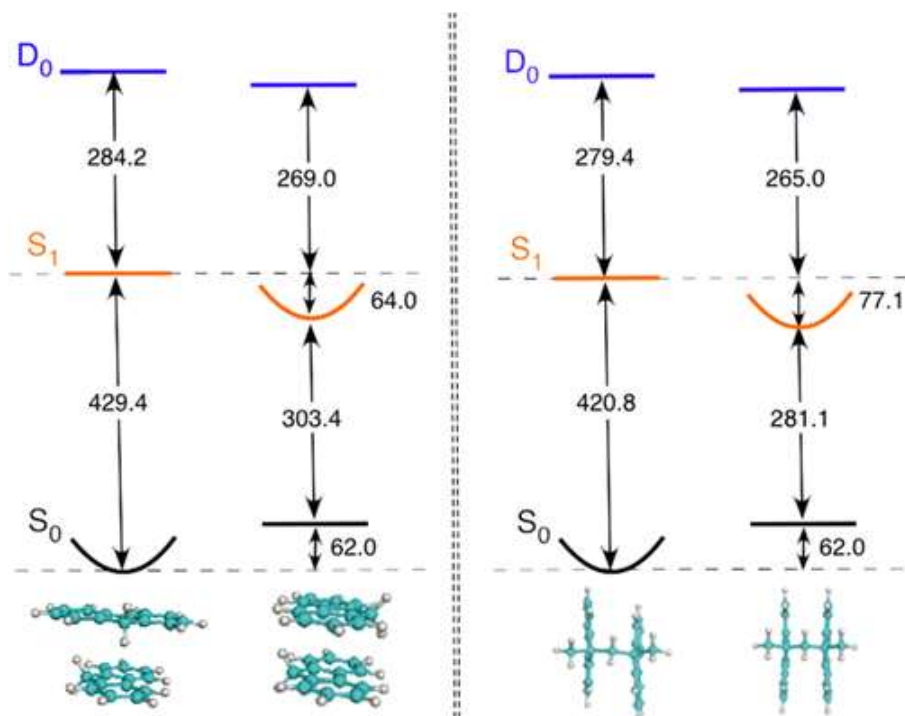

Figure 4. Calculated points on the potential energy surfaces of $(F)_2$ (at left) and F2. Parabolas indicate where geometry optimizations were performed.

For the covalently linked F2, the ground state minimum is a cofacial parallel–displaced structure, and the excimer lies ~77 kJ/mol below the vertical energy of the LE state. The increased stabilization of the F2 excimer, by some 25%, as predicted by theory is roughly consistent with the observed experimental red-shift of the excimeric emission relative to $(F)_2$, Figure 2. Vertical ionization of F2 requires 342 kJ/mol of energy from the bottom of the excimer well. Thus, our calculations support the experimental finding that the excimeric state is stabilized in the covalently linked dimer, whereas the vertical ionization energies of the two dimers are predicted to be similar.

Additional insights are provided from study of the van der Waals dimer of F1; that is, the 9,9'-dimethyl derivative, details of which will be reported in a future publication. As shown in Figure 2 in the SI, gas-phase emission spectra of $(F1)_2$ show beautifully resolved torsional structure which affords ready assignment to the head-to-tail π-stacked dimer. *Surprisingly, there is no evidence of excimeric emission*! This is rationalized as due to the increased steric constraints imposed by the methyl substituents, which prevents a sandwich overlap of the chromophores. In contrast, the measured IP of $(F1)_2$ is 7.58(1) eV, which lies above that of F2 and $(F)_2$ but still evidence significant stabilization relative to the monomer.

These findings highlight the diverse geometrical requirements inherent to excimer formation vs cation radical stabilization in a π-stacked bichromophore, which we have explored by exploiting the fact that processes of ionization and emission occur from the (same) excimeric state in the isolated molecules. Excimer formation, which is dominated by exciton resonance and π-stacking, is favored by a perfect "sandwich" overlap of the two chromophores.[30] This is maximal in the covalently linked dimer, whereas steric constraints lead the van der Waals dimer to stack in a head-to-tail arrangement (Figure 4). The geometrical requirements for cation radical stabilization, which involves significant charge transfer, are less restrictive.

In organic-based electronic devices, excimer formation serves to trap generated excitons, hindering charge separation. Understanding the geometrical requirements for excimer formation vs hole stabilization thus provides valuable insights for the design of new multichromophoric assemblies.

Author Present Address

(N.R.) Department of Chemistry, University of Massachusetts—Boston, Boston, MA 02125.

The authors declare no competing financial interest.

Acknowledgment

References

[1]Hoeben, F. J.; Jonkheijm, P.; Meijer, E. W.; Schenning, A. P.About Supramolecular Assemblies of Π-Conjugated Systems *Chem. Rev.* 2005, 105, 1491– 1546, DOI: 10.1021/cr030070z

[2]Hirata, T.; Ikeda, H.; Saigusa, H.Dynamics of Excimer Formation and Relaxation in the T-Shaped Benzene Dimer *J. Phys. Chem. A* 1999, 103, 1014– 1024, DOI: 10.1021/jp983814z

[3]Balmer, F. A.; Trachsel, M. A.; van der Avoird, A.; Leutwyler, S.The Elusive S2 State, the S1/S2 Splitting, and the Excimer States of the Benzene Dimer J. Chem. Phys. 2015, 142, 234306, DOI: 10.1063/1.4922608

[4]Saigusa, H.; Lim, E. C.Localized and Delocalized Excited States of the Fluorene Dimers J. Phys. Chem. 1991, 95, 1194– 1200, DOI: 10.1021/j100156a030

[5]Wessel, J.; Beck, S.; Highstrete, C.Excitonic Interaction in the Fluorene Dimer J. Chem. Phys. 1994, 101, 10292– 10302, DOI: 10.1063/1.467909

[6]Saigusa, H.; Lim, E. C.Excimer Formation in Van Der Waals Dimers and Clusters of Aromatic Molecules Acc. Chem. Res. 1996, 29, 171– 178, DOI: 10.1021/ar950169v

[7]Duhamel, J.New Insights in the Study of Pyrene Excimer Fluorescence to Characterize Macromolecules and Their Supramolecular Assemblies in Solution Langmuir 2012, 28, 6527– 6538, DOI: 10.1021/la2047646

[8]Chipot, C.; Jaffe, R.; Maigret, B.; Pearlman, D. A.; Kollman, P. A.Benzene Dimer: A Good Model for Π-Π Interactions in Proteins? A Comparison between the Benzene and the Toluene Dimers in the Gas Phase and in

Journal of Physical Chemistry Letters, Vol 7, No. 15 (August 4, 2016): pg. 3042-3045. [DOI]. This article is © American Chemical Society and permission has been granted for this version to appear in e-Publications@Marquette. American Chemical Society does not grant permission for this article to be further copied/distributed or hosted elsewhere without the express permission from American Chemical Society.

9

an Aqueous Solution J. Am. Chem. Soc. 1996, 118, 11217– 11224, DOI: 10.1021/ja961379l

[9]Amicangelo, J. C.Theoretical Study of the Benzene Excimer Using Time-Dependent Density Functional Theory J. Phys. Chem. A 2005, 109, 9174– 9182, DOI: 10.1021/jp053445o

[10]Sinnokrot, M. O.; Sherrill, C. D.High-Accuracy Quantum Mechanical Studies of Pi-Pi Interactions in Benzene Dimers J. Phys. Chem. A 2006, 110, 10656– 10668, DOI: 10.1021/jp0610416

[11]Hunter, C. A.; Sanders, J. K.The Nature of Pi-Pi Interactions J. Am. Chem. Soc. 1990, 112, 5525– 5534, DOI: 10.1021/ja00170a016

[12]Martinez, C. R.; Iverson, B. L.Rethinking the Term Pi-Stacking Chemical Science 2012, 3, 2191– 2201, DOI: 10.1039/c2sc20045g

[13]Rathore, R.; Abdelwahed, S. H.; Guzei, I. A.Synthesis, Structure, and Evaluation of the Effect of Multiple Stacking on the Electron-Donor Properties of Pi-Stacked Polyfluorenes J. Am. Chem. Soc. 2003, 125, 8712– 8713, DOI: 10.1021/ja035518s

[14]Rathore, R.; Chebny, V. J.; Abdelwahed, S. H.A Versatile and Conformationally Adaptable Fluorene-Based Receptor for Efficient Binding of Silver Cation J. Am. Chem. Soc. 2005, 127, 8012– 8013, DOI: 10.1021/ja051935o

[15]Rathore, R.; Abdelwahed, S. H.; Kiesewetter, M. K.; Reiter, R. C.; Stevenson, C. D.Intramolecular Electron Transfer in Cofacially Pi-Stacked Fluorenes: Evidence of Tunneling J. Phys. Chem. B 2006, 110, 1536– 1540, DOI: 10.1021/jp052737m

[16]Chebny, V. J.; Rathore, R.Convergent Synthesis of Alternating Fluorene-P-Xylene Oligomers and Delineation of the (Silver) Cation-Induced Folding J. Am. Chem. Soc. 2007, 129, 8458– 8465, DOI: 10.1021/ja0687522

[17]Nakano, T.Synthesis, Structure and Function of Π-Stacked Polymers Polym. J. 2010, 42, 103– 123, DOI: 10.1038/pj.2009.332

[18]Vura-Weis, J.; Abdelwahed, S. H.; Shukla, R.; Rathore, R.; Ratner, M. A.; Wasielewski, M. R.Crossover from Single-Step Tunneling to Multistep Hopping for Molecular Triplet Energy Transfer Science 2010, 328, 1547– 1550, DOI: 10.1126/science.1189354

[19]Miyazaki, M.; Fujii, M.Real Time Observation of the Excimer Formation Dynamics of a Gas Phase Benzene Dimer by Picosecond Pump-Probe Spectroscopy Phys. Chem. Chem. Phys. 2015, 17, 25989– 25997, DOI: 10.1039/C5CP03010B

[20]Navale, T. S.; Thakur, K.; Vyas, V. S.; Wadumethrige, S. H.; Shukla, R.; Lindeman, S. V.; Rathore, R.Charge Delocalization in Self-Assembled Mixed-Valence Aromatic Cation Radicals Langmuir 2012, 28, 71– 83, DOI: 10.1021/la202611w

[21]Sinnokrot, M. O.; Sherrill, C. D.Highly Accurate Coupled Cluster Potential Energy Curves for the Benzene Dimer: Sandwich, T-Shaped, and Parallel-Displaced Configurations J. Phys. Chem. A 2004, 108, 10200– 10207, DOI: 10.1021/jp0469517

[22]Perdew, J. P.; Ernzerhof, M.; Burke, K.Rationale for Mixing Exact Exchange with Density Functional Approximations J. Chem. Phys. 1996, 105, 9982– 9985, DOI: 10.1063/1.472933

[23]Adamo, C.; Barone, V.Accurate Excitation Energies from Time-Dependent Density Functional Theory: Assessing the PBE0 Model for Organic Free Radicals Chem. Phys. Lett. 1999, 314, 152– 157, DOI: 10.1016/S0009-2614(99)01113-6

[24]Grimme, S.; Antony, J.; Ehrlich, S.; Krieg, H.A Consistent and Accurate Ab Initio Parametrization of Density Functional Dispersion Correction (Dft-D) for the 94 Elements H-Pu J. Chem. Phys. 2010, 132, 154104, DOI: 10.1063/1.3382344

[25]Weigend, F.; Ahlrichs, R.Balanced Basis Sets of Split Valence, Triple Zeta Valence and Quadruple Zeta Valence Quality for H to Rn: Design and Assessment of Accuracy Phys. Chem. Chem. Phys. 2005, 7, 3297– 3305, DOI: 10.1039/b508541a

[26]Weigend, F.Accurate Coulomb-Fitting Basis Sets for H to Rn Phys. Chem. Chem. Phys. 2006, 8, 1057– 1065, DOI: 10.1039/b515623h

[27]Renz, M.; Theilacker, K.; Lambert, C.; Kaupp, M.A Reliable Quantum-Chemical Protocol for the Characterization of Organic Mixed-Valence Compounds J. Am. Chem. Soc. 2009, 131, 16292– 16302, DOI: 10.1021/ja9070859

[28]Renz, M.; Kess, M.; Diedenhofen, M.; Klamt, A.; Kaupp, M.Reliable Quantum Chemical Prediction of the Localized/Delocalized Character of Organic Mixed-Valence Radical Anions. From Continuum Solvent Models to Direct-Cosmo-Rs J. Chem. Theory Comput. 2012, 8, 4189– 4203, DOI: 10.1021/ct300545x

[29]Talipov, M. R.; Boddeda, A.; Timerghazin, Q. K.; Rathore, R.Key Role of End-Capping Groups in Optoelectronic Properties of Poly-P-Phenylene Cation Radicals J. Phys. Chem. C 2014, 118, 21400– 21408, DOI: 10.1021/jp5082752

[30]Talipov, M. R.; Ivanov, M. V.; Reid, S. A.; Rathore, R.Two's Company, Three's a Crowd: Exciton Localization in Cofacially Arrayed Polyfluorenes J. Phys. Chem. Lett. 2016, 2915– 2920, DOI: 10.1021/acs.jpclett.6b01268

Supporting Information

The Supporting Information is available free of charge on the <u>ACS Publications website</u> at DOI: <u>10.1021/acs.jpclett.6b01201</u>.

- Materials and methods; potential energy surface profiles for $(F)_2$, F2 and F2H2; S_1/S_2 states and V_{ab} coupling; additional references. (<u>PDF</u>)

Supporting Information

First Experimental Evidence for the Diverse Requirements of Excimer vs. Hole Stabilization in π-Stacked Assemblies

Neil Reilly,[‡] Maxim Ivanov, Brandon Uhler, Marat Talipov, Rajendra Rathore*, and Scott A. Reid*

Department of Chemistry, Marquette University, P. O. Box 1881, Milwaukee, WI 53233

Corresponding Author
* Rajendra Rathore (rajendra.rathore@marquette.edu);
Scott A. Reid (scott.reid@marquette.edu)

Table of contents:

Materials and Methods

<u>Experimental</u> <u>Details</u>

Our experiments utilized two different machines, equipped with identical heat supersonic molecular beam sources, for Resonant 2-photon ionization (R2PI)[1] and laser induced fluorescence (LIF) studies. The R2PI experiments were conducted in a linear 1 m time-of-flight mass spectrometer (TOFMS). A sample (typically 0.1-1%) of the species of interest in a rare gas (He or Ar) was generating by passing the gas through a heated solid sample cartridge which contained roughly 50 mg of the compound of interest trapped between loosely packed plugs of glass wool. The sample cartridge and nozzle, a solenoid-actuated pulsed valve (Parker-Hannifin), were heated up to temperatures of ~ 250°C using a flexible heater element; separate thermocouples were used to monitor their temperatures. The mixture was expanded at a total pressure of typically ~ 1-2 bar from the 1.0 mm diameter nozzle, and the resulting gas pulse, of ~ 1 ms duration, passed through a 1.0 mm diameter skimmer into the differentially pumped flight tube of a one-meter linear time-of-flight mass spectrometer. The flight tube vacuum was maintained by a 250 L/s turbomolecular pump, and a gate valve used to isolate the detector, which was kept under vacuum at all times. The main chamber was evacuated with a water-baffled diffusion pump (Varian VHS-4). With the nozzle on, typical pressures were ~ 5 x 10^{-5} mbar (main chamber) and ~ 1 x 10^{-6} mbar (flight tube). The background pressure in the flight tube could be lowered further by liquid nitrogen cooling of the vacuum shroud. Several types of resonant ionization experiments were conducted. First, mass-selected excitation spectra were obtained using a 1+1 R2PI scheme, with laser light near 300 nm generated by frequency doubling in a BBO crystal the output of a dye laser (Lambda-Physik, Scanmate 2E), pumped by the second harmonic of an Nd:YAG laser (Continuum NY-61). Typical output pulse energies were 1–2 mJ in the doubled beam, which was loosely focused with a 1.0 or 2.0 m plano-convex lens into the chamber. Ions were extracted and accelerated using a conventional three-plate stack, with the repeller plate typically held at +2100 V, the extractor plate at +1950 V, and the third plate at ground potential. The ions traversed a path of 1 m prior to striking a dual chevron microchannel plate detector. The detector signal was amplified (x 20) using a fast preamplifier (Femto HVA-500M-20B), and integrated using a boxcar system (Stanford Research SRS250) interfaced to a personal computer. An in-house LABVIEW program controlled data acquisition and stepped the laser wavelength; typically, the signal from twenty laser shots was averaged at each step in wavelength.

Once the mass-selected excitation spectrum was obtained using 1+1 R2PI, a second frequency doubled dye laser system (Sirah Cobra-Stretch pumped by second harmonic of Spectra-Physics INDI laser) was employed to perform two-color R2PI (i.e, 1+1' R2PI or 2CR2PI) experiments on species of interest. Here, the timing of the two lasers was controlled using an 8-channel digital pulse/delay generator (Berkeley Nucleonics 565), and the conditions (focusing, energy, temporal and spatial overlap) were optimized to enhance the ratio of 2-photon to 1-photon signal. To determine ionization potentials, the excitation laser was tuned to the origin of the species of interest, and the ionization laser was scanned through the ionization threshold.

Hole-burning experiments were conducted to probe for the existence of multiple conformers. In these experiments, the third harmonic (355 nm) of a Continuum Minilite II Nd:YAG laser was used as the ionizing laser, and the INDI/Sirah system was employed as the holeburning laser, the frequency of which was set to a specific feature in the spectrum of interest. Using the divide by *n* feature of the pulse generator, the Nd:YAG Q-switch of this laser was toggled at a repetition rate of 5 Hz, or a duty cycle ½ that of the nozzle and ionization laser(s), and the Q-switch delays was set so that the hole-burning laser preceded the ionizing (probe) laser(s) in time by 100-500 ns. The hole-burning spectrum was obtained using active subtraction on a shot-by-shot basis, where each shot obtained with only the ionizing (probe) laser(s) fired were subtracted from the preceding shot, where all lasers were fired. The subtracted signal was averaged over typically 20 laser shots, and recorded as the probe laser was scanned.

Laser induced fluorescence experiments were conducted in a separate chamber equipped with an identical molecular beam source. For these experiments we used the INDI/Sirah system. The timing of laser and nozzle firing was controlled by a four–channel digital pulse/delay generator (Berkeley Nucleonics model 575). The laser beam was not focused, and typical pulse energies were ~ 0.5–1 mJ in a ~ 3 mm diameter beam. These measurements utilized a mutually orthogonal geometry of laser, molecular beam, and detector, where the laser beam crossed the molecular beam at a distance of ~ 15 mm (19 nozzle diameters) downstream. Fluorescence was collected and collimated by a *f*/2.4 plano-convex lens, and focused using a second 2 in dia. *f*/3.0 lens either: (a) through a long-pass cutoff filter onto a photomultiplier tube detector (PMT, Oriel 77348) for monitoring total fluorescence, or (b) onto the slit of a 0.55 m monochromator/spectrograph (Horiba iHR550) equipped with a PMT detector (Oriel 77348). Fluorescence excitation spectra were acquired by integrating the PMT output using a gated integrator (Stanford Research SR250). The integrator output was digitized by a 12 bit ADC (Measurement Computing USB-1208FS), and passed to a computer for analysis. Typically, the signal was averaged over twenty laser shots at each step in wavelength. Data collection and laser wavelength and monochromator control was achieved using LABVIEW software.
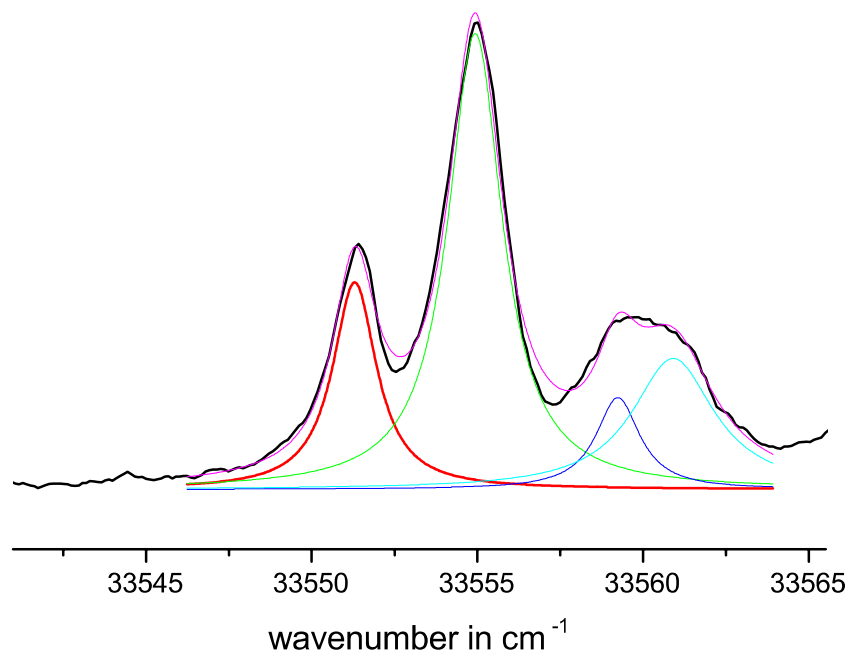
Figure S1. Lorentzian fits to the lowest energy features in the spectrum of the fluorene dimer. The origin feature is well fit by a Lorentzian with a linewidth of 1.6 cm^{-1}, indicating a timescale of several ps for excimer formation.
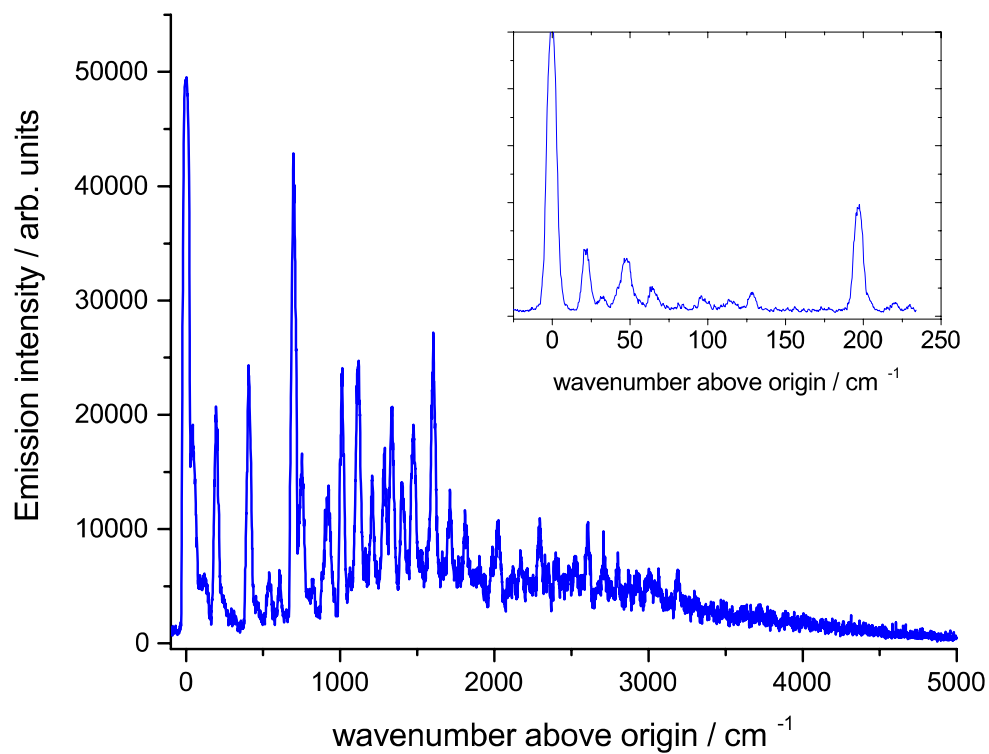
Figure S2. Emission spectra of the van der Waals dimer of 9,9'-dimethylfluorene (F1).
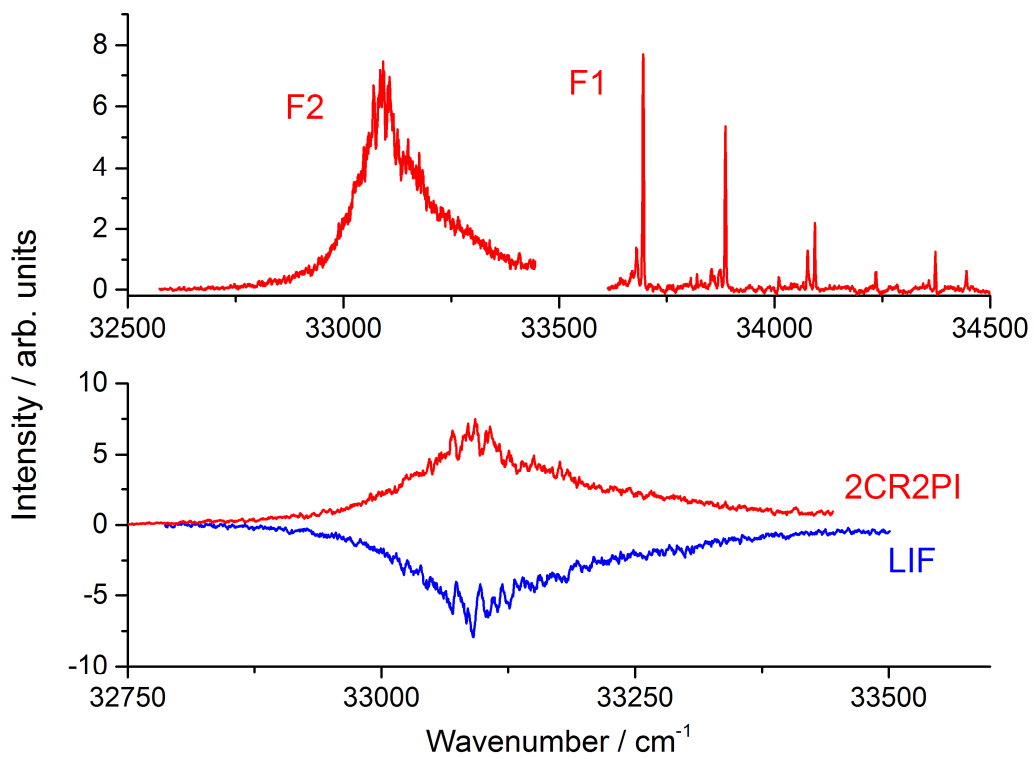
Figure S3. R2PI and LIF spectra of covalently linked F2, compared with F1.

Computational details

All electronic structure calculations of F2H2, F2 and $(F)_2$ were performed with the Gaussian 09 package, revision D01.[2] Due to the importance of the electronic correlation in the proper description of π-π interactions, we performed a brief benchmarking study to evaluate several density functional theory (DFT) and *ab initio* methods on the example of benzene dimer in its sandwich, parallel and T-shape configurations.[3] We found that accurate energy of π-π stacking of two benzene molecules could be obtained by using a simple PBE0 density functional[4,5] augmented with D3 version of Grimme's dispersion term[6] only at a fraction of the computational cost of more sophisticated methods (Table S1). This observation is in agreement with the recent comprehensive benchmark study on the example of benzene-naphthalene complex.[7] Thus, ground electronic state calculations of F2H2, F2 and $(F)_2$ were performed using DFT with PBE0 functional, D3 version of Grimme's dispersion and def2-TZVP basis set.[8,9] Excited electronic states were computed using the time-dependent density functional theory (TD-DFT)[10,11] method with D3 version of Grimme's dispersion at def2-TZVP and def2-SV(P) basis sets. For vertically ionized cationic states of F2H2, F2 and $(F)_2$ we used calibrated[12-14] B1LYP functional[15] that contains 40% contribution (denoted as B1LYP-40) of the exact exchange with 6-31G(d) basis set.[16] The wave function stability tests were performed to ensure absence of solutions with lower energy.[17,18] The values of $<S^2>$ operator after spin annihilation were confirmed to be close to the expectation value of 0.75, thus indicating that spin contamination was not an issue for the performed calculations. To confirm that the structures correspond to the minimum on the ground and excited electronic PES we performed geometry optimizations and Hessian matrix calculations at PBE0-D3/def2-SV(P) level of theory. In all DFT calculations, ultrafine Lebedev's grid was used with 99 radial shells per atom and 590 angular points in each shell. Tight cutoffs on forces and atomic displacement were used to determine convergence in geometry optimization procedure. The nudged elastic band (NEB)[19] method was used to estimate the upper boundary of the transition state between tilted orthogonal and sandwich structures on the first excited (S1) PES (Figure S3). NEB was used as implemented in DL-FIND code[20] with the in-house developed interface to split NEB images calculations across the nodes of computational cluster.[21]

Table S1. Benchmarking of different methods to compute interaction energy in benzene dimer (in kcal/mol). Calculations at CCSD(T)/aug-cc-pVQZ were taken as a reference.[3]

Theory	Sandwich	Parallel	T-shaped	RMSD
CCSD(T)/aug-cc-pVQZ	-1.7	-2.62	-2.61	-
CCSD/6-31G(d)	-1.95	-3.08	-3.33	0.51
CCSD/cc-pVDZ	-0.58	-1.46	-2.37	0.95
CCSD-F12a/aug-cc-pVDZ	-1.3	-2.19	-2.51	0.35
CCSD-F12b/aug-cc-pVDZ	-1.17	-2.05	-2.46	0.46
CCSD-F12a/aug-cc-pVTZ	-0.86	-1.71	-2.2	0.75
CCSD-F12b/aug-cc-pVTZ	-0.9	-1.77	-2.27	0.71
CCSD(T)-F12a/ aug-cc-pVDZ	-2.37	-3.47	-3.4	0.77
CCSD(T)-F12b/aug-cc-pVDZ	-2.24	-3.33	-3.36	0.67
CCSD(T)-F12a/aug-cc-pVTZ	-1.95	-2.96	-3.01	0.33
CCSD(T)-F12b/aug-cc-pVTZ	-1.99	-3.02	-3.08	0.39
M062x/aug-cc-pVDZ	-1.65	-3.48	-3.18	0.6
PBE0-D3/6-311+G(d,f)	-2.25	-3.54	-3.64	0.86
PBE0-D3/def2-SVP	-2.29	-3.33	-3.44	0.72
PBE0-D3/def2-TZVP	-1.73	-2.68	-3.05	0.26
PBE0-D3/def2-TZVPP	-1.73	-2.65	-3.00	0.23
PBE0-D3/def2-TZVPPD	-1.78	-2.64	-2.97	0.21
wB97XD/aug-cc-pVDZ	-2.60	-4.06	-3.68	1.16
B3LYP/aug-cc-pVDZ	2.24	1.68	-0.08	3.67
SAPT0/aug-cc-pVDZ	-1.14	-2.37	-2.52	0.36
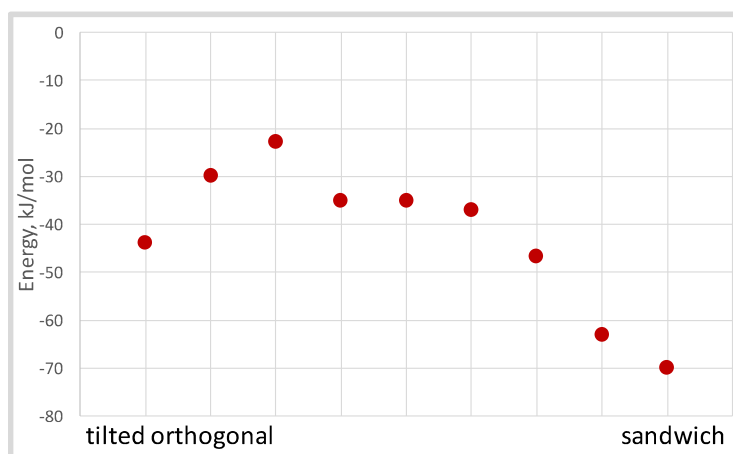
Figure S3. Nudged elastic band pathway between tilted orthogonal and sandwich structures on the excited (S$_1$) PES using PBE0-D3/def-SV(P). Energies are in kcal/mol relative to the vertically excited energy of the parallel orthogonal structure.

Potential energy surface profiles for (F)₂, F2 and F2H2
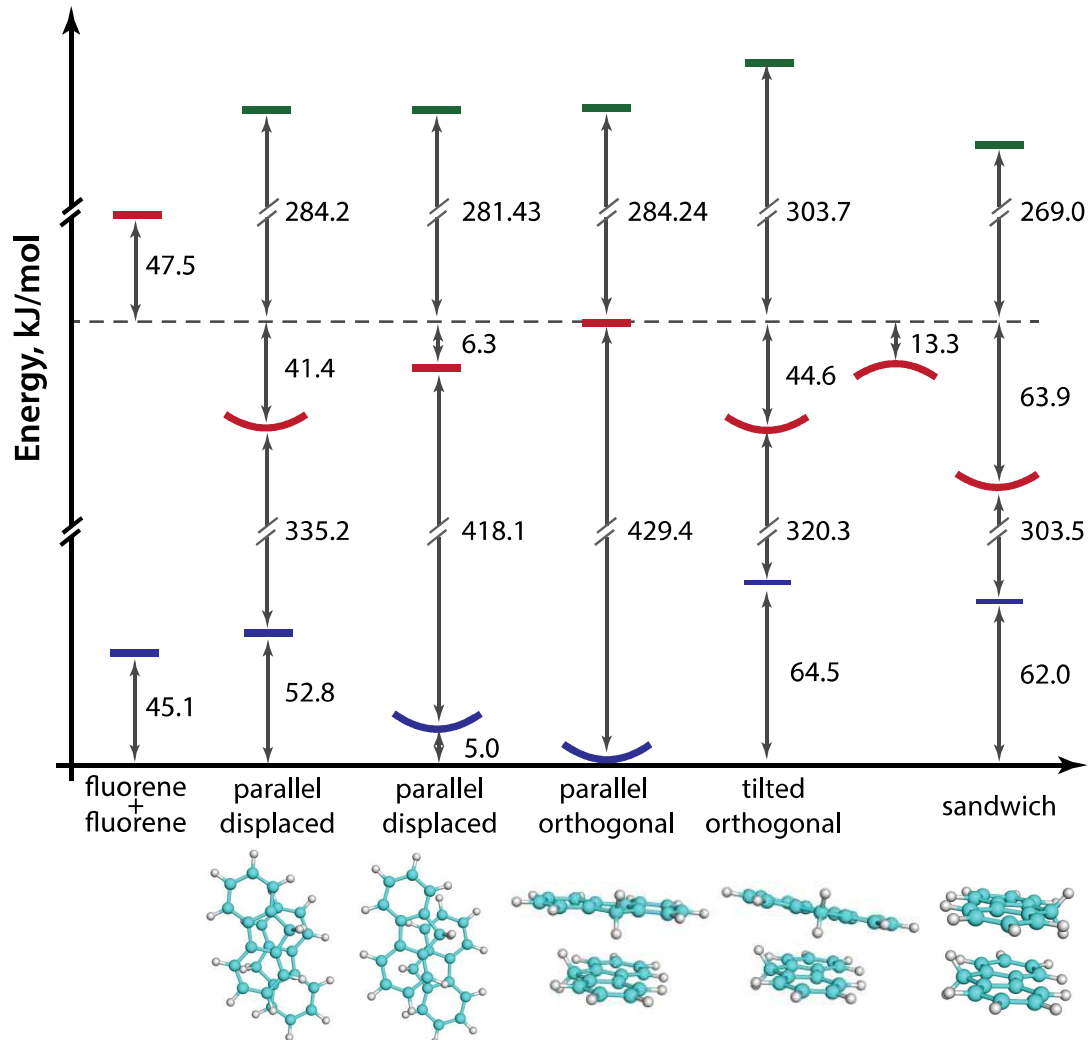
Figure S4. Calculated stationary points of the fluorene dimer, (F)₂, in ground (S0), first excited (S1) and ionized (D0) state using PBE0-D3/def2-TZVP.
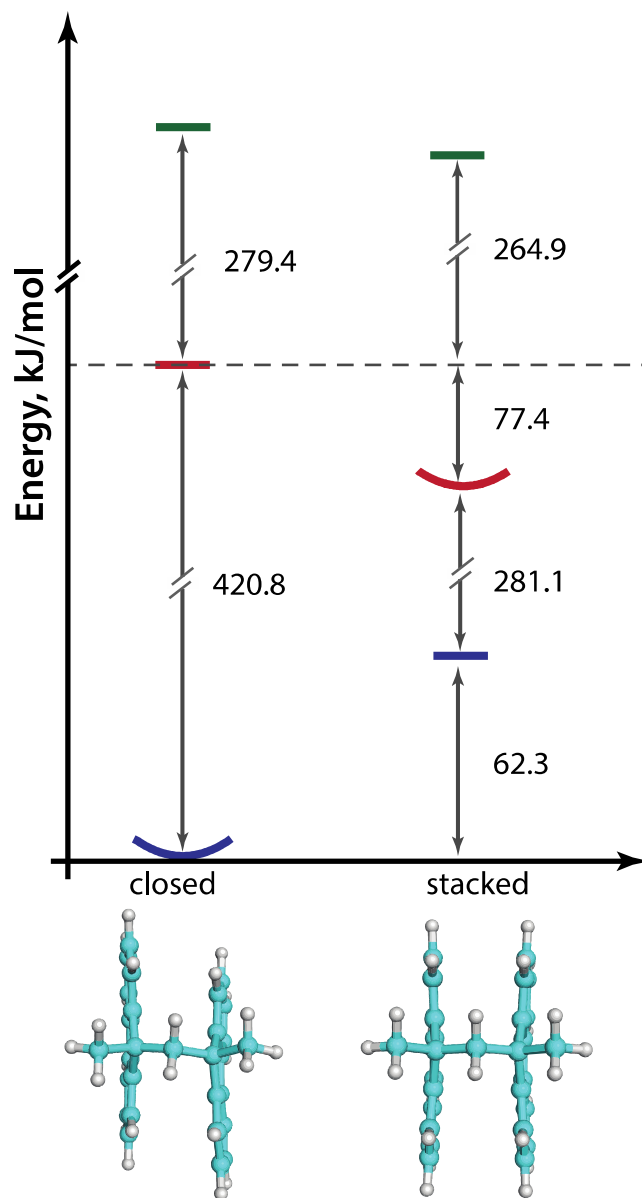
Figure S5. Calculated stationary points of F2 in ground (S_0), first excited (S_1) and ionized (D_0) state using PBE0-D3/def2-TZVP.
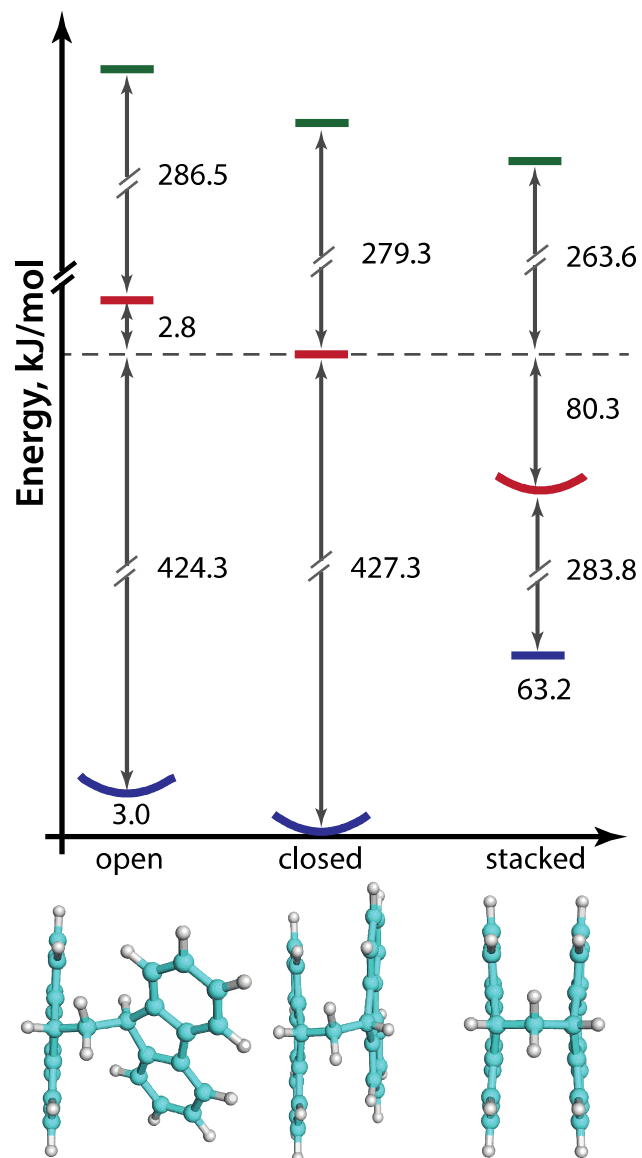
Figure S6. Calculated stationary points of F2H2 in ground (S_0), first excited (S_1) and ionized (D_0) state using PBE0-D3/def2-TZVP.

Table S2. Energies of ground (S_0), excited (S_1) and cationic (D_0) states of $(F)_2$ calculated at PBE0-D3/def2-TZVP level of theory relative to the energy of parallel orthogonal structure (global minimum on ground electronic state). All values are in kJ/mol.

	F+F*	parallel displaced S1	parallel displaced S0	parallel orthogonal	tilted orthogonal	TS	sandwich
D0	782.4	713.6	710.8	713.6	733.1		698.4
S1	477.0	388.0	423.1	429.4	384.8	416.2	365.5
S0	45.1	52.8	5.0	0.0	64.5	47.7	62.0

Table S3. Energies of ground (S_0), excited (S_1) and cationic (D_0) states of $(F)_2$ calculated at PBE0-D3/def2-SV(P) level of theory relative to the energy of parallel orthogonal structure (global minimum on ground electronic state). All values are in kJ/mol.

	F+F*	parallel displaced S1	parallel displaced S0	parallel orthogonal	tilted orthogonal	TS	sandwich
D0	795.2	715.3	713.0	715.2	738.6		696.6
S1	491.2	387.6	427.0	434.3	382.5	411.4	364.1
S0	53.6	56.6	6.5	0.0	76.3	35.4	62.2

Table S4. Energies of ground (S_0), excited (S_1) and cationic (D_0) states of $(F)_2$ calculated at BLYP40/6-31G(d) level of theory relative to the energy of parallel orthogonal structure (global minimum on ground electronic state). All values are in kJ/mol.

	F+F*	parallel displaced S1	parallel displaced S0	parallel orthogonal	tilted orthogonal	TS	sandwich
D0	705.7	683.7	682.5	685.2	690.4		680.2
S1	453.3	432.1	467.3	471.9	434.3		420.7
S0	5.2	48.3	-2.3	0.0	40.3		68.4

Table S5. Energies of ground ground (S_0), excited (S_1) and cationic (D_0) states of F2H2 calculated at PBE0-D3/def2-TZVP level of theory relative to the energy of the closed structure (global minimum on ground electronic state). All values are in kJ/mol.

	closed	open	stacked
D0	706.6	716.7	690.9
S1	427.3	430.2	347.0
S0	0.0	3.0	63.2

Table S6. Energies of ground (S_0), excited (S_1) and cationic (D_0) states of F2H2 calculated at PBE0-D3/def2-SV(P) level of theory relative to the energy of the closed structure (global minimum on ground electronic state). All values are in kJ/mol.

	closed	open	stacked
D0	705.2	724.7	691.0
S1	425.9	439.8	346.8
S0	0.0	9.4	64.0

Table S7. Energies of ground (S_0), excited (S_1) and cationic (D_0) states of F2H2 calculated at BLYP40/6-31G(d) level of theory relative to the energy of the closed structure (global minimum on ground electronic state). All values are in kJ/mol.

	closed	open	stacked
D0	678.9	677.0	665.8
S1	465.7	456.2	395.6
S0	0.0	-12.4	64.3

Table S8. Energies of ground (S_0), excited (S_1) and cationic (D_0) states of F2 calculated at PBE0-D3/def2-TZVP level of theory relative to the energy of the closed structure. All values are in kJ/mol.

	closed	stacked
D0	700.2	685.7
S1	420.8	343.4
S0	0.0	62.3

Table S9. Energies of ground (S_0), excited (S_1) and cationic (D_0) states of F2 calculated at PBE0-D3/def2-SV(P) level of theory relative to the energy of the closed structure. All values are in kJ/mol.

	closed	stacked
D0	699.0	686.0
S1	420.7	343.8
S0	0.0	63.8

Table S10. Energies of ground (S_0), excited (S_1) and cationic (D_0) states of F2 calculated at BLYP40/6-31G(d) level of theory relative to the energy of the closed structure. All values are in kJ/mol.

	closed	stacked
D0	678.7	660.2
S1	460.9	391.2
S0	0.0	63.0

S₁/S₂ states and V_ab coupling

Tables below contain the energy of states S_1 and S_2 relative to the S_0 state for the corresponding geometry, coupling V_{ab}, oscillator strength f for each transition, number of orbitals involved in the transition and corresponding coefficients.

Table S11. F2 closed conformation at TD PBE0-GD3/def2-TZVP

	E, eV	E, kJ/mol	f	transition	coeff.
S₁	4.361	420.8	0.0080	99 -> 100	0.68185
				98 -> 100	0.52189
S₂	4.452	429.6	0.0155	98 -> 102	-0.11376
				99 -> 101	-0.4496
V_ab	0.046	4.4			

Table S12. F2 stacked conformation at TD PBE0-GD3/def2-TZVP

	E, eV	E, kJ/mol	f	transition	coeff.
S₁	2.914	281.2	0.0000	99 -> 100	-0.7048
S₂	3.480	335.7	0.0000	96 -> 100	0.16872
				99 -> 101	-0.68259
V_ab	0.283	27.3			

Table S13. F2 closed conformation at TD PBE0-GD3/def2-SV(P)

	E, eV	E, kJ/mol	f	transition	coeff.
S₁	4.3602	420.7	0.0064	99 -> 100	0.68318
				98 -> 100	0.50821
S₂	4.4625	430.6	0.0161	98 -> 102	0.11735
				99 -> 101	0.46014
V_ab	0.051	4.9			

Table S14. F2 stacked conformation at TD PBE0-GD3/def2-SV(P)

	E, eV	E, kJ/mol	f	transition	coeff.
S₁	2.903	280.1	0.0000	99 -> 100	0.70496
S₂	3.524	340.0	0.0000	97 -> 100	-0.20779
				99 -> 101	-0.67134
V_ab	0.311	30.0			

Table S15. F2 closed conformation at BLYP40/6-31G(d)

	E, eV	E, kJ/mol	f	transition	coeff.
S₁	4.777	460.9	0.0292	98 -> 100	0.5473

	E, eV	E, kJ/mol	f	transition	coeff.
				99 -> 101	-0.40158
				94 -> 100	-0.12657
				96 ->101	-0.10767
S_2	4.902	473.0	0.4483	96 ->103	0.1037
				98 ->101	-0.44226
				99 ->100	0.45431
				99 ->102	0.16183
V_{ab}	0.062	6.0			

Table S16. F2 stacked conformation at BLYP40/6-31G(d)

	E, eV	E, kJ/mol	f	transition	coeff.
S_1	3.402	328.2	0.000	99 -> 100	0.70055
S_2	4.083	393.9	0.000	96 -> 100	0.22527
				99 -> 101	0.65369
V_{ab}	0.341	32.9			

Table S17. F2H2 closed conformation at TD PBE0-GD3/def2-TZVP

	E, eV	E, kJ/mol	f	transition	coeff.
S_1	4.429	427.3	0.0097	90 -> 92	0.67692
				90 -> 93	-0.40695
				90 -> 95	-0.10213
S_2	4.460	430.3	0.0082	91 -> 92	0.44265
				91 -> 94	-0.3342
V_{ab}	0.015	1.5			

Table S18. F2H2 open conformation at TD PBE0-GD3/def2-TZVP

	E, eV	E, kJ/mol	f	transition	coeff.
S_1	4.427	427.1	0.0259	91 -> 92	0.69982
				86 -> 92	0.14388
				88 -> 92	0.11401
				88 -> 93	-0.12438
				90 -> 92	0.40918
S_2	4.592	443.1	0.0629	90 -> 93	0.19802
				90 -> 94	0.20976
				91 -> 93	-0.23746
				91 -> 94	0.28089
				91 -> 95	0.17168
V_{ab}	0.083	8.0			

Table S19. F2H2 stacked conformation at TD PBE0-GD3/def2-TZVP

	E, eV	E, kJ/mol	f	transition	coeff.
S_1	2.943	283.9	0.0000	91 -> 92	0.70474
S_2	3.403	328.3	0.0000	88 -> 92	0.14146
				91 -> 93	0.68904
V_{ab}	0.230	22.2			

Table S20. F2H2 closed conformation at TD PBE0-GD3/def2-SV(P)

	E, eV	E, kJ/mol	f	transition	coeff.
S1	4.414	425.9	0.0072	91 -> 92	0.68437
S2	4.472	431.5	0.0138	90 -> 92	0.50745
				90 -> 94	0.23193
				91 -> 93	0.40925
Vab	0.029	2.8			

Table S21. F2H2 open conformation at TD PBE0-GD3/def2-SV(P)

	E, eV	E, kJ/mol	f	transition	coeff.
S1	4.461	430.4	0.0263	91 -> 92	0.70089
S2	4.664	450.0	0.1021	86 -> 92	0.12853
				88 -> 92	0.13176
				88 -> 93	-0.11806
				90 -> 92	0.48891
				90 -> 93	0.11338
				90 -> 94	0.15406
				91 -> 93	-0.27263
				91 -> 94	0.20394
				91 -> 95	-0.15107
Vab	0.102	9.8			

Table S22. F2H2 stacked conformation at TD PBE0-GD3/def2-SV(P)

	E, eV	E, kJ/mol	f	transition	coeff.
S_1	2.932	282.9	0.0000	91 -> 92	0.70479
S_2	3.468	334.6	0.0000	88 -> 92	-0.17679
				91 -> 93	0.68031
V_{ab}	0.268	25.8			

Table S23. F2H2 closed conformation at BLYP40/6-31G(d)

	E, eV	E, kJ/mol	f	transition	coeff.
S_1	4.827	465.7	0.0365	90 -> 92	0.54521
				91 -> 93	-0.40578

	E, eV	E, kJ/mol	f	transition	coeff.
				86 -> 92	0.16762
				88 -> 93	-0.19085
S₂	4.940	476.6	0.001	90 -> 93	0.18966
				90 -> 95	-0.26658
				91 -> 92	0.26013
				91 -> 94	0.48633
Vab	0.057	5.5			

Table S24. F2H2 open conformation at BLYP40/6-31G(d)

	E, eV	E, kJ/mol	f	transition	coeff.
				90 -> 92	0.36036
S₁	4.857	468.6	0.1012	90 -> 93	0.12218
				91 -> 92	-0.34584
				91 -> 93	0.43929
				86 -> 92	-0.13227
				86 -> 94	0.10773
				90 -> 92	0.51468
S₂	4.930	475.7	0.4861	90 -> 93	0.14800
				90 -> 94	0.10537
				91 -> 92	0.18210
				91 -> 93	-0.32144
Vab	0.037	3.5			

Table S25. F2H2 stacked conformation at BLYP40/6-31G(d)

	E, eV	E, kJ/mol	f	transition	coeff.
S₁	2.742	264.6	0.000	90 -> 94	-0.12836
S₂	3.186	307.4	0.000	91 -> 92	0.6935
				88 -> 92	-0.18015
				91 -> 93	0.67923
Vab	0.222	21.4			

Table S26. (F)₂ tilted orthogonal conformation at TD PBE0-GD3/def2-TZVP

	E, eV	E, kJ/mol	f	transition	coeff.
S₁	3.320	320.4	0.0357	88 -> 89	0.70335
S₂	3.718	358.8	0.0654	87 -> 89	-0.68184
				88 -> 90	0.15911
Vab	0.199	19.2			

Table S27. (F)₂ tilted orthogonal conformation at TD PBE0-GD3/def-SV(P)

	E, eV	E, kJ/mol	f	transition	coeff.
S_1	3.173	306.2	0.0304	88 -> 89	-0.70413
S_2	3.661	353.2	0.056	87 -> 89	0.67832
				88 -> 90	-0.17576
V_{ab}	0.244	23.5			

Table S28. (F)$_2$ tilted orthogonal conformation at BLYP40/6-31G(d)

	E, eV	E, kJ/mol	f	transition	coeff.
S_1	4.083	394.0	0.1738	88 -> 89	0.69557
S_2	4.393	423.9	0.1069	87 -> 89	-0.68628
V_{ab}	0.155	14.9			

Table S29. (F)$_2$ sandwich conformation at TD PBE0-GD3/def2-TZVP

	E, eV	E, kJ/mol	f	transition	coeff.
S_1	3.145	303.5	0.0000	88 -> 89	-0.70494
				85 -> 89	0.18232
S_2	3.865	372.9	0.0213	88 -> 90	0.61715
				88 -> 91	0.26988
V_{ab}	0.360	34.7			

Table S30. (F)$_2$ TD sandwich conformation at PBE0-GD3/def2-SV(P)

	E, eV	E, kJ/mol	f	transition	coeff.
S_1	3.130	302.0	0.0000	88 -> 89	0.70509
				85 -> 89	-0.18865
S_2	3.860	372.5	0.0328	88 -> 90	0.63599
				88 -> 91	0.22034
V_{ab}	0.365	35.3			

Table S31. (F)$_2$ sandwich conformation at BLYP40/6-31G(d)

	E, eV	E, kJ/mol	f	transition	coeff.
S_1	3.652	352.3	0.0000	88 -> 89	0.70121
				85 -> 89	-0.17886
S_2	4.330	417.8	0.0548	88 -> 90	0.60182
				88 -> 91	0.29136
V_{ab}	0.339	32.7			

Table S32. (F)$_2$ parallel displaced S1 conformation at TD PBE0-GD3/def2-TZVP

	E, eV	E, kJ/mol	f	transition	coeff.
S$_1$	3.652	352.3	0.0000	88 -> 89	0.70121
				85 -> 89	-0.17886
S$_2$	4.330	417.8	0.0548	88 -> 90	0.60182
				88 -> 91	0.29136
V$_{ab}$	0.302	29.2			

Table S33. (F)$_2$ parallel displaced S1 conformation at TD PBE0-GD3/def2-SV(P)

	E, eV	E, kJ/mol	f	transition	coeff.
S$_1$	3.430	331.0	0.0000	88 -> 89	0.70322
S$_2$	4.085	394.1	0.0018	87 -> 89	-0.4989
				88 -> 90	0.48149
V$_{ab}$	0.327	31.6			

Table S34. (F)$_2$ parallel displaced S1 conformation at BLYP40/6-31G(d)

	E, eV	E, kJ/mol	f	transition	coeff.
S$_1$	3.978	383.8	0.0000	88 -> 89	0.69431
				87 -> 89	-0.57423
S$_2$	4.634	447.1	0.7097	88 -> 90	0.36056
				88 -> 91	0.10227
V$_{ab}$	0.328	31.7			

Table S35. (F)$_2$ parallel displaced S0 at TD PBE0-GD3/def2-TZVP

	E, eV	E, kJ/mol	f	transition	coeff.
S$_1$	4.333	418.1	0.0000	88 -> 89	0.68598
				87 -> 89	0.63532
				87 -> 91	-0.14154
S$_2$	4.592	443.1	0.2092	88 -> 90	-0.11391
				88 -> 92	-0.17842
V$_{ab}$	0.129	12.5			

Table S36. (F)$_2$ parallel displaced S0 at TD PBE0-GD3/def2-SV(P)

	E, eV	E, kJ/mol	f	transition	coeff.
S$_1$	4.358	420.5	0.0000	88 -> 89	0.69044
S$_2$	4.631	446.9	0.1153	87 -> 89	0.6209
				88 -> 90	-0.29672
V$_{ab}$	0.137	13.2			

Table S37. (F)$_2$ parallel displaced S0 at BLYP40/6-31G(d)

	E, eV	E, kJ/mol	f	transition	coeff.
S$_1$	4.867	469.6	0.0000	87 -> 90	0.32979
				88 -> 89	0.57413
				83 -> 90	-0.11755
				84 -> 89	-0.12246
				84 -> 91	0.1038
S$_2$	4.968	479.3	0.5755	87 -> 89	0.44965
				87 -> 91	0.14914
				88 -> 90	0.42248
				88 -> 92	-0.15043
V$_{ab}$	0.050	4.9			

Table S38. (F)$_2$ parallel orthogonal at TD PBE0-GD3/def2-TZVP

	E, eV	E, kJ/mol	f	transition	coeff.
S1	4.451	429.4	0.0622	87 -> 90	-0.11811
				87 -> 92	0.10413
				88 -> 89	0.66232
				88 -> 91	-0.11351
S2	4.466	430.9	0.0662	87 -> 89	0.65419
				87 -> 91	-0.10521
				88 -> 90	-0.16696
Vab	0.008	0.8			

Table S39. (F)$_2$ parallel orthogonal at TD PBE0-GD3/def2-SV(P)

	E, eV	E, kJ/mol	f	transition	coeff.
S1	4.501	434.3	0.0494	87 -> 90	0.1927
				88 -> 89	0.65135
S2	4.515	435.6	0.0444	87 -> 89	0.63633
				88 -> 90	0.24853
Vab	0.007	0.7			

Table S40. (F)$_2$ parallel orthogonal at BLYP40/6-31G(d)

	E, eV	E, kJ/mol	f	transition	coeff.
S1	4.891	471.9	0.2302	84 -> 89	0.10817
				87 -> 90	-0.28858
				87 -> 92	0.10686
				88 -> 89	0.59097
S2	4.897	472.5	0.257	87 -> 89	0.59209
				88 -> 90	-0.2771
				88 -> 92	0.11635
Vab	0.003	0.3			

References

(1)   Dietz, T. G.; Duncan, M. A.; Liverman, M. G.; Smalley, R. E. *J Chem Phys* **1980**, *73*, 4816.

(2)   Frisch, M. J.; Trucks, G. W.; Schlegel, H. B.; Scuseria, G. E.; Robb, M. A.; Cheeseman, J. R.; Scalmani, G.; Barone, V.; Mennucci, B.; Petersson, G. A.; Nakatsuji, H.; Caricato, M.; Li, X.; Hratchian, H. P.; Izmaylov, A. F.; Bloino, J.; Zheng, G.; Sonnenberg, J. L.; Hada, M.; Ehara, M.; Toyota, K.; Fukuda, R.; Hasegawa, J.; Ishida, M.; Nakajima, T.; Honda, Y.; Kitao, O.; Nakai, H.; Vreven, T.; Montgomery, J., J. A.; Peralta, J. E.; Ogliaro, F.; Bearpark, M.; Heyd, J. J.; Brothers, E.; Kudin, K. N.; Staroverov, V. N.; Keith, T.; Kobayashi, R.; Normand, J.; Raghavachari, K.; Rendell, A.; Burant, J. C.; Iyengar, S. S.; Tomasi, J.; Cossi, M.; Rega, N.; Millam, J. M.; Klene, M.; Knox, J. E.; Cross, J. B.; Bakken, V.; Adamo, C.; Jaramillo, J.; Gomperts, R.; Stratmann, R. E.; Yazyev, O.; Austin, A. J.; Cammi, R.; Pomelli, C.; Ochterski, J. W.; Martin, R. L.; Morokuma, K.; Zakrzewski, V. G.; Voth, G. A.; Salvador, P.; Dannenberg, J. J.; Dapprich, S.; Daniels, A. D.; Farkas, O.; Foresman, J. B.; Ortiz, J. V.; Cioslowski, J.; Fox, D. J. In *Gaussian 09, Revision D.01*; Gaussian, Inc., Wallingford CT: 2010.

(3)   Sinnokrot, M. O.; Sherrill, C. D. *J Phys Chem A* **2004**, *108*, 10200.

(4)   Perdew, J. P.; Ernzerhof, M.; Burke, K. *J Chem Phys* **1996**, *105*, 9982.

(5)   Adamo, C.; Barone, V. *J Chem Phys.* **1999**, *110*, 6158.

(6)   Grimme, S.; Antony, J.; Ehrlich, S.; Krieg, H. *J Chem Phys* **2010**, *132*, 154104.

(7)   Wang, W.; Sun, T.; Zhang, Y.; Wang, Y.-B. *J Chem Phys* **2015**, *143*, 114312.

(8)   Weigend, F. *Phys Chem Chem Phys* **2006**, *8*, 1057.

(9)   Weigend, F.; Ahlrichs, R. *Phys Chem Chem Phys* **2005**, *7*, 3297.

(10)   Casida, M. E.; Jamorski, C.; Casida, K. C.; Salahub, D. R. *J Chem Phys* **1998**, *108*, 4439.

(11)   Stratmann, R. E.; Scuseria, G. E.; Frisch, M. J. *J Chem Phys* **1998**, *109*, 8218.

(12)   Talipov, M. R.; Boddeda, A.; Timerghazin, Q. K.; Rathore, R. *J Phys Chem C* **2014**, *118*, 21400.

(13)   Renz, M.; Kess, M.; Diedenhofen, M.; Klamt, A.; Kaupp, M. *J Chem Theory Comput* **2012**, *8*, 4189.

(14)   Renz, M.; Theilacker, K.; Lambert, C.; Kaupp, M. *J Am Chem Soc* **2009**, *131*, 16292.

(15)   Adamo, C.; Barone, V. *Chem Phys Lett* **1997**, *274*, 242.

(16)   Hehre, W. J.; Ditchfield, R.; Pople, J. A. *J Chem Phys* **1972**, *56*, 2257.

(17)   Bauernschmitt, R.; Ahlrichs, R. *J Chem Phys* **1996**, *104*, 9047.

(18)   Seeger, R.; Pople, J. A. *J Chem Phys* **1977**, *66*, 3045.

(19)   Jónsson, H.; Mills, G.; Jacobsen, K. W. **1998**.

(20)   Kästner, J.; Carr, J. M.; Keal, T. W.; Thiel, W.; Wander, A.; Sherwood, P. *J Phys Chem A* **2009**, *113*, 11856.

(21)   Ivanova, L. V.; Anton, B. J.; Timerghazin, Q. K. *Phys Chem Chem Phys* **2014**, *16*, 8476.